# The viscous lee wave problem and its implications for ocean modelling

Callum J. Shakespeare[a,b,*], Andrew McC. Hogg[a,b]

[a] *Research School of Earth Sciences, Australian National University, Canberra, Australian Capital Territory.*
[b] *Australian Research Council Centre of Excellence for Climate System Science*

**Abstract**

Ocean circulation models employ horizontal viscosity and diffusivity to represent unresolved sub-gridscale processes such as breaking internal waves. Computational power has now advanced sufficiently to permit regional ocean circulation models to be run at sufficiently high (100m-1km) horizontal resolution to resolve a significant part of the internal wave spectrum. Here we develop theory for boundary generated internal waves in such models, and in particular, where the waves dissipate their energy. We focus specifically on the steady lee wave problem where stationary waves are generated by a large-scale flow acting across ocean bottom topography. We generalise the energy flux expressions of Bell (1975) to include the effect of horizontal viscosity and diffusivity. Applying these results for realistic parameter choices we show that in the present generation of models with $O(1)m^2s^{-1}$ horizontal viscosity/diffusivity boundary-generated waves will inevitably dissipate the majority of their energy within a few hundred metres of the boundary. This

*Corresponding Author: *Phone*: +61 2 6125 4517
*Email address:* callum.shakespeare@anu.edu.au (Callum J. Shakespeare)

dissipation is essentially spurious since it is a direct consequence of the artificially high viscosity/diffusivity used in the numerical models and hence caution is necessary in comparing model results to ocean observations. Our theory further predicts that $O(0.01)m^2s^{-1}$ horizontal viscosity/diffusivity is required to satisfactorily reduce the spurious dissipation and enable a realistic representation of wave dynamics in ocean models.

*Keywords:* internal waves, dissipation, lee waves

## 1. Introduction

Internal waves are an important mechanism for vertical and downscale transfer of energy in the ocean. Internal waves can transport energy from the upper and lower boundary of the ocean (where much of the energy is injected) to the ocean interior, where wave breaking and other nonlinear processes can lead to turbulent mixing (Waterhouse et al., 2014). Furthermore, they are amongst the larger scales of 'unbalanced' flow, and can therefore provide a conduit from large-scale 'balanced' flow to the small-scale turbulence where dissipation occurs (Vanneste, 2013). Internal waves are generated by surface wind stresses (Watson et al., 1976), tidal interactions with bathymetry (e.g. St Laurent and Garrett, 2002), geostrophic flows over rough topography on the sea floor (Nikurashin and Ferrari, 2010), and small-scale unbalanced flow at the ocean surface including submesoscale eddies, fronts and filaments (e.g. Danioux et al., 2012; Nagai et al., 2015; Shakespeare and Taylor, 2016).

Only recently have computational capabilities expanded sufficiently to permit regional ocean circulation models to be run at sufficiently high (100m-1km) horizontal resolution to resolve a significant portion of the internal wave

spectrum (Nikurashin et al., 2013; Nagai et al., 2015; Rosso et al., 2015). In their 200m resolution model, Nikurashin et al. (2013) find that the resolved waves generated via geostrophic flow over topography (lee waves) dissipate 80% of their energy in the water column directly above the topography. They extrapolate this result to the global ocean to suggest that the resolved waves with scales exceeding 1km provide a first-order contribution to turbulent mixing directly above topography, thereby sustaining the ocean overturning circulation. Enhanced dissipation above rough topography is consistent with ocean observations (Waterhouse et al., 2014). However, observational estimates suggest that lee waves only dissipate 2-20% of their energy near topography (Waterman et al., 2013), much less than the 80% predicted from the Nikurashin et al. (2013) numerical model.

As with all large-scale ocean models, the subgrid-scale turbulence in wave-resolving numerical models must be parameterised, typically using Laplacian (or higher order) horizontal diffusivities and/or viscosities. The fact that the horizontal gridscale (100m-1km) is much larger than the vertical (1-20m) implies that the corresponding viscosity/diffusivity will be that much larger: typical values of Laplacian horizontal diffusivities and/or viscosities employed in these high resolution models (e.g. Nikurashin et al., 2013; Nagai et al., 2015; Rosso et al., 2015) are of $O(1)\mathrm{m}^2\ \mathrm{s}^{-1}$ throughout the depth of the ocean. In comparison, values for vertical viscosity/diffusivity are typically of $O(10^{-3} - 10^{-5})\mathrm{m}^2\ \mathrm{s}^{-1}$. To some extent these parameterisations are intended to represent the effect of internal waves breaking and driving mixing of density and momentum in the ocean interior (Polzin, 2010; Polzin and Lvov, 2011). This situation presents a problem since we are parameterising

the effect of waves while partially resolving waves, and thus any effect the parameterisation has on the waves is essentially a spurious one. Here we investigate this effect and what can be done to minimise or eliminate it.

The 'fluid' in the numerical models described above (which we will term the 'model fluid') has strongly non-isotropic behaviour, with horizontal viscosity/diffusivity dominating over the vertical for typical internal wave aspect ratios. Further, most of these models use the hydrostatic version of the Boussinesq equations, so we will only consider hydrostatic internal waves. Thus, our objective here is formulate hydrostatic linear internal wave theory to describe the energy flux associated with boundary-sourced internal waves in the presence of horizontal viscosity/diffusivity. In particular, we will extend the classic steady lee wave energy flux expression of Bell (1975), which has been recently used to estimate lee wave generation in the global ocean (e.g. Nikurashin et al., 2014), to include viscous and diffusive effects. We describe this as the 'viscous lee wave problem'.

## 2. Linear wave theory

Here we investigate the dynamics of internal waves generated at a boundary in a 'model fluid' with purely horizontal viscosity and/or diffusivity using linear theory. The hydrostatic Boussinesq equations with uniform Laplacian horizontal diffusivity ($\kappa_h$) and viscosity ($A_h$) on an $f$-plane, linearised about a state with uniform barotropic, time-independent background flow,

$\mathbf{U} = (U, V, 0)$, and constant stratification, $N^2$, are

$$\begin{aligned}
\frac{\partial u}{\partial t} - fv + \mathbf{U} \cdot \nabla_h u &= -\frac{1}{\rho_0}\frac{\partial p}{\partial x} + A_h \nabla_h^2 u, && \text{(1a)}\\
\frac{\partial v}{\partial t} + fu + \mathbf{U} \cdot \nabla_h v &= -\frac{1}{\rho_0}\frac{\partial p}{\partial y} + A_h \nabla_h^2 v, && \text{(1b)}\\
0 &= -\frac{1}{\rho_0}\frac{\partial p}{\partial z} + b, && \text{(1c)}\\
\frac{\partial b}{\partial t} + wN^2 + \mathbf{U} \cdot \nabla_h b &= \kappa_h \nabla_h^2 b, && \text{(1d)}\\
0 &= \frac{\partial u}{\partial x} + \frac{\partial v}{\partial y} + \frac{\partial w}{\partial z}, && \text{(1e)}
\end{aligned}$$

where $(u, v, w)$ are the velocities in the $(x, y, z)$ Cartesian coordinate directions, $p$ is the pressure, $b = -g(\rho - \rho_0)/\rho_0$ the buoyancy, $f$ the Coriolis parameter, and $\rho_0$ the reference density. We seek solutions to (1) with the form of plane waves moving with the background flow,

$$\begin{aligned}
b &= \widehat{b}(k, l, \omega, z) \exp\left(\imath(k(x - Ut) + l(y - Vt) + \omega t)\right)\\
&= \widehat{b}(k, l, \Omega, z) \exp\left(\imath(kx + ly + \Omega t)\right), && \text{(2)}
\end{aligned}$$

where $\imath = \sqrt{-1}$, $k$, $l$ are the $x$ and $y$ wavenumbers, $\omega$ the Lagrangian frequency, and $\Omega = \omega - (kU + lV)$ the Doppler shifted (Eulerian) frequency. Our objective here is to determine the vertical structure function, $\widehat{b}(k, l, \omega, z)$, which describes the vertical amplitude profile of a wave, given the scale and frequency. Similar expressions to (2) apply for the velocity and pressure

fields. Substituting these expressions into (1) yields,

$$\widehat{b} = \widehat{b_0}\, e^{\gamma(z-z_b)}, \tag{3a}$$

$$\widehat{p} = \rho_0 \int \widehat{b}\, dz, \tag{3b}$$

$$\widehat{u} = \frac{\imath l(\imath\omega - K^2 A_h) + \imath k f}{f^2 + (\imath\omega - K^2 A_h)^2} \frac{\widehat{p}}{\rho_0}, \tag{3c}$$

$$\widehat{v} = \frac{\imath k(\imath\omega - K^2 A_h) - \imath l f}{f^2 + (\imath\omega - K^2 A_h)^2} \frac{\widehat{p}}{\rho_0}, \tag{3d}$$

$$\widehat{w} = \frac{1}{N^2}(\imath\omega - K^2\kappa_h)\widehat{b}, \tag{3e}$$

where

$$\gamma^2 = \frac{K^2 N^2\,(\imath\omega - A_h K^2)}{(f^2 + (\imath\omega - A_h K^2)^2)\,(\imath\omega - K^2\kappa_h)}. \tag{4}$$

The sign of $\gamma$ must be chosen such that solutions decay as away from the boundary ($z = z_b$). The function $\widehat{b}_0(k, l, \omega)$ is the boundary condition on the buoyancy due to the forcing mechanism (e.g. topography, buoyancy flux; see below). We now introduce appropriately defined Reynolds, $\mathrm{Re} = \omega/(A_h K^2)$, and Peclet, $\mathrm{Pe} = \omega/(\kappa_h K^2)$, numbers to describe the relative strength of the horizontal viscosity and diffusivity. The solution to (4) in terms of these non-dimensional numbers is

$$\gamma = \pm NK\imath\sqrt{\frac{(1 - \imath\mathrm{Re})\mathrm{RePe}}{(1 - \imath\mathrm{Pe})(\omega^2(\imath + \mathrm{Re})^2 - f^2\mathrm{Re}^2)}}. \tag{5}$$

Most model fluids are in a weakly viscous and diffusive limit in which $\mathrm{Re} \gg 1$ and $\mathrm{Pe} \gg 1$. In this limit, (5) becomes

$$\gamma = \pm\left(\imath m + \left(\frac{1}{h_\kappa} + \frac{1}{h_A}\right)\right), \tag{6}$$

where $m$ is the vertical wave number (when $\omega > f$),

$$m = \frac{NK}{\sqrt{\omega^2 - f^2}}, \tag{7}$$

$h_\kappa$ is the diffusive decay depth,

$$h_\kappa = \frac{2\mathrm{Pe}\sqrt{\omega^2 - f^2}}{NK}, \tag{8}$$

and $h_A$ is the viscous decay depth,

$$h_A = \frac{2\mathrm{Re}(\omega^2 - f^2)^{3/2}}{NK(\omega^2 + f^2)}. \tag{9}$$

Thus, in the weakly viscous scenario the wavenumber ($m$) is unaffected by viscous effects, but there is a potentially significant decay of propagating wave ($\omega > f$) amplitudes away from the boundary where they are generated. The total decay depth, $h$, is the geometric mean of the viscous and diffusive decay depths,

$$h = \left(\frac{1}{h_\kappa} + \frac{1}{h_A}\right)^{-1} = \frac{2\omega\sqrt{\omega^2 - f^2}}{NK^3}\left(\kappa_h + \frac{\omega^2 + f^2}{|\omega^2 - f^2|}A_h\right)^{-1}. \tag{10}$$

The decay depth in the weakly viscous limit is always very much larger than the vertical wavelength, $\lambda = 2\pi/m$; for example, $h_\kappa/\lambda = \mathrm{Pe}/\pi \gg 1$. The non-wave or geostrophic part of the solution ($\omega < f$) is characterised by an imaginary vertical wavenumber $m$ (7). Independent of the viscosity or diffusivity, frequencies $\omega < f$ therefore decay rapidly away from the boundary with inviscid decay depth $\lambda/(2\pi) = 1/|m| = \sqrt{f^2 - \omega^2}/(NK)$. The viscous and diffusive decay depth defined by (10) is imaginary (wavelike) for $\omega < f$, but since $\lambda \ll |h|$ in the weakly viscous limit, the geostrophic flow decays sufficiently rapidly that the viscous and diffusive contributions can be neglected. As will be shown below, this result does *not* imply that there is no energy dissipated from the geostrophic ($\omega < f$) flow, only that the loss is not sufficient to substantially affect its amplitude.

The amount of energy lost by both waves and geostrophic flow at a given vertical level may be computed by forming the energy budget. The equation for the time evolution of kinetic energy, $E_K = (u^2 + v^2)/2$, is obtained by multiplying (1a) by $u$, (1b) by $v$, summing the two equations, and then integrating in $x$ and $y$ to yield

$$\frac{\partial \langle E_K \rangle}{\partial t} = -\frac{1}{\rho_0}\frac{\partial}{\partial z}\langle wp \rangle + \langle wb \rangle - A_h \langle |\nabla_h \mathbf{u}_h|^2 \rangle, \tag{11}$$

where angled brackets $\langle\rangle$ denote the horizontal average. Similarly, the equation for the time evolution of available potential energy (APE), $E_A = b^2/(2N^2)$, is obtained by multiplying (1d) by $b$, dividing by $N^2$, and then integrating in $x$ and $y$ to yield

$$\frac{\partial \langle E_A \rangle}{\partial t} = -\langle wb \rangle - \frac{\kappa_h}{N^2}\langle |\nabla_h b|^2 \rangle. \tag{12}$$

The total perturbation energy, $E = E_K + E_A$, thus evolves according to

$$\begin{aligned} \frac{\partial \langle E \rangle}{\partial t} &= -\frac{1}{\rho_0}\frac{\partial}{\partial z}\langle wp \rangle - A_h \langle |\nabla_h \mathbf{u}_h|^2 \rangle - \frac{\kappa_h}{N^2}\langle |\nabla_h b|^2 \rangle \\ &= -\frac{\partial F}{\partial z} - \epsilon - \phi_i. \end{aligned} \tag{13}$$

Thus at steady state the decay of the energy flux $F$ with height corresponds to a deposition of energy either via viscous dissipation, $\epsilon$, or irreversible mixing, $\phi_i$. Using Parseval's theorem we can compute this energy deposition as an integral over all wavenumbers and appropriate frequencies,

$$\phi_i = \frac{\kappa_h}{(2\pi)^3 N^2} \int\int\int K^2 |\widehat{b}|^2 \, dk \, dl \, d\omega, \tag{14}$$

and

$$\begin{aligned} \epsilon = &\quad \frac{A_h}{(2\pi)^3} \int\int\int K^2 \left( |\widehat{u}|^2 + |\widehat{v}|^2 \right) \, dk \, dl \, d\omega \\ \simeq &\quad \frac{A_h}{(2\pi)^3 N^2} \int\int\int K^2 \zeta \frac{\omega^2 + f^2}{|\omega^2 - f^2|} |\widehat{b}|^2 \, dk \, dl \, d\omega, \end{aligned} \tag{15}$$

substituting the solution (3), and taking the weakly viscous limit. The parameter $\zeta$ in (15),

$$\zeta = \left(1 + \frac{2K^4 A_h^2(\omega^2 + f^2)}{(\omega^2 - f^2)^2}\right)^{-\frac{1}{2}}, \tag{16}$$

is important only to prevent infinities at near inertial frequencies, $|\omega/f - 1| \leq \mathrm{Re}^{-2}$, and may otherwise be neglected. The net energy deposition, $D = \epsilon + \phi_i$, from the wave flow (i.e. integral over $\omega > f$) is

$$D_w = \frac{1}{(2\pi)^3 N^2} \int_f^\infty \int\int K^2 \left(\kappa_h + \zeta \frac{\omega^2 + f^2}{\omega^2 - f^2} A_h\right) e^{-\frac{2|z - z_b|}{h}} |\widehat{b}_0(k, l, \omega)|^2 \, dk \, dl \, d\omega, \tag{17}$$

where $h$ is the viscous/diffusive wave decay depth (10). Similarly, the net energy deposition from the non-wave geostrophic flow (i.e. integral over $0 < \omega < f$) is

$$D_m = \frac{1}{(2\pi)^3 N^2} \int_0^f \int\int K^2 \left(\kappa_h + \zeta \frac{\omega^2 + f^2}{f^2 - \omega^2} A_h\right) e^{-2|z - z_b||m|} |\widehat{b}_0(k, l, \omega)|^2 \, dk \, dl \, d\omega, \tag{18}$$

where $1/|m|$ is the geostrophic decay depth, as described above. The wave energy flux at a given depth, $F_w = |wp|/\rho_0$, can now be computed as the vertical integral (e.g. (13)) of the net energy deposition defined by (17),

$$F_w(z) = \frac{1}{(2\pi)^3} \int_f^\infty \int\int \frac{\omega\sqrt{\omega^2 - f^2}}{N^3 K} e^{-\frac{2|z - z_b|}{h}} |\widehat{b}_0(k, l, \omega)|^2 \, dk \, dl \, d\omega. \tag{19}$$

Similarly, the energy flux associated with the geostrophic non-wave flow is

$$F_m(z) = \frac{1}{(2\pi)^3} \int_0^f \int\int \frac{K\sqrt{f^2 - \omega^2}}{2N^3} \left(\kappa_h + \zeta \frac{\omega^2 + f^2}{f^2 - \omega^2} A_h\right) e^{-2|z - z_b||m|} \, |\widehat{b}_0(k, l, \omega)|^2 \, dk \, dl \, d\omega. \tag{20}$$

The above results can describe many different mechanisms of wave forcing at boundaries through an appropriate choice of $\widehat{b}_0(k, l, \omega)$. We consider the particular case of steady lee waves in the next section.

*Steady lee waves*

Lee waves are generated by large-scale flow over topography in a stratified fluid. The linearised boundary condition is that flow is parallel to the topography, or $w = \mathbf{U}_h \cdot \nabla_h H$, where $H(x, y)$ is the height of the bottom topography above $z = 0$. For small amplitude topography, the boundary condition is applied at $z = 0$ and thus $\widehat{w}_0 = (-\imath kU - \imath lV)\widehat{H}$, or in terms of buoyancy

$$\widehat{b}_0(k, l, \omega) = \frac{N^2 \widehat{w}_0}{\imath\omega - \kappa_h K^2} \simeq \frac{-N^2 \widehat{H}\,(kU + lV)}{\omega}, \tag{21}$$

assuming the fluid is weakly diffusive (Pe $\gg 1$), as previously. For *steady* lee waves we require the Eulerian frequency $\Omega = \omega - (kU + lV) = 0$, and thus the Lagrangian frequency is $\omega = (kU + lV)$ and (21) becomes

$$\widehat{b}_0(k, l, \omega) = -N^2 \widehat{H}\, 2\pi\delta(\omega - (kU + lV)), \tag{22}$$

where $\delta$ is the Dirac delta function. Substituting (22) into (19) and, without loss of generality, choosing our $x$-axis to coincide with the local flow, the lee wave energy flux is

$$F_w = \frac{1}{(2\pi)^2} \int \int_{f/U}^{\infty} NU \frac{k}{K} \sqrt{k^2U^2 - f^2} e^{-\frac{2z}{h}} |\widehat{H}|^2 \, dk \, dl, \tag{23}$$

where

$$h = \frac{2kU\sqrt{k^2U^2 - f^2}}{NK^3} \left( \kappa_h + \frac{k^2U^2 + f^2}{k^2U^2 - f^2} A_h \right)^{-1}. \tag{24}$$

Equation (23) agrees with the usual expression (e.g. Bell, 1975) for the hydrostatic steady lee wave energy flux at $z = 0$, but unlike the classical inviscid/adiabatic problem, the flux decays with height over $e$-folding scale $h/2$. Similarly, substituting (22) into (20) yields the energy flux associated with

dissipation from the non-wave flow (i.e. the geostrophic flow around topography) for the steady lee wave problem. This flux is identically zero in the classical inviscid problem.

To understand the implications of the above results for ocean modelling we need to make appropriate choices for free-stream speed $U$, stratification $N^2$, Coriolis frequency $f$ and the topographic height spectrum $|\widehat{H}|^2$. Here we will use parameters characteristic of the Drake Passage region of the Southern Ocean: $N^2 = 10^{-6}\mathrm{s}^{-2}$ and $f = -1.2\times10^{-4}\mathrm{s}^{-1}$. Goff and Jordan (1988) show that the height spectrum of sea floor topography may be well approximated by

$$|\widehat{H}(k,l)|^2 = \frac{2\pi H_{rms}^2(\mu-2)}{k_0 l_0}\left[1+\frac{K^2}{k_0^2}\cos^2(\phi-\phi_0)+\frac{K^2}{l_0^2}\sin^2(\phi-\phi_0)\right]^{-\mu/2}, \tag{25}$$

where $k_0$ and $l_0$ are the characteristic easterly and northerly wavenumbers, $\phi$ is the angle of the wavevector with respect to east, $H_{rms}$ is the root-mean-square topographic height, $\phi_0$ is the azimuthal angle and $\mu$ characterises the roll-off of the spectrum at high wavenumbers. Here we will use the same parameter values as Nikurashin and Ferrari (2010): $H_{rms} = 305\mathrm{m}$, $\mu = 3.5$, $k_0 = 2.3\times10^{-4}\mathrm{m}^{-1}$, $l_0 = 1.3\times10^{-4}\mathrm{m}^{-1}$ and $\phi_0 = 320^\circ$. Figure 1 displays the net energy deposition from the wave (solid) and geostrophic (dotted) flow given the above parameter choices, for three different free-stream speeds: (a) 2cm $\mathrm{s}^{-1}$, (b) 5cm $\mathrm{s}^{-1}$ and (c) 10cm $\mathrm{s}^{-1}$. Each plot shows the result for three different choices of turbulent parameters: both viscosity and diffusivity ($A_h = \kappa_h = 1\mathrm{m}^2\ \mathrm{s}^{-1}$; blue), viscosity only ($A_h = 1\mathrm{m}^2\ \mathrm{s}^{-1}$; red) and diffusivity only ($\kappa_h = 1\mathrm{m}^2\ \mathrm{s}^{-1}$; black). These turbulent parameters are comparable to those used in recent high resolution modelling studies (e.g. Nikurashin et al.,

2013, use $A_h = 1\mathrm{m}^2\ \mathrm{s}^{-1}$ and $\kappa_h \simeq 0$).

We first consider the energy deposition from the geostrophic flow (dotted curves). The geostrophic flow energy loss is essentially independent of the free-stream speed and also of whether viscosity or diffusivity is responsible (red and black dotted curves overlap). This behaviour results from the rapid roll-off of the topographic spectrum (25) with wavenumber such that near-inertial frequencies (wavenumbers $k \sim f/U$) do not contribute significantly to the geostrophic flow energy loss: with this assumption, the geostrophic flow energy deposition (18) may be expressed as

$$D_m = N^2(\kappa_h + A_h)\left[\frac{1}{(2\pi)^2}\int_{-\infty}^{\infty}\int_{0}^{\infty} K^2|\widehat{H}|^2 e^{-\frac{2NK}{|f|}z}\,dk\,dl\right]. \qquad (26)$$

The energy deposition at the boundary ($z = 0$) is thus $3(\kappa_h + A_h) \times 10^{-8}\mathrm{W}$ $\mathrm{kg}^{-1}$ for the present parameters and the vast majority of the geostrophic flow energy loss will occur within $h_m = |f|/(2Nk_0) \sim 260\mathrm{m}$ of the boundary, consistent with figure 1. The total dissipation of geostrophic flow energy is the vertical integral of (26),

$$\rho_0\int_0^{\infty} D_m\,dz = \frac{1}{2}\rho_0 N|f|(\kappa_h + A_h)\left[\frac{1}{(2\pi)^2}\int_{-\infty}^{\infty}\int_{0}^{\infty} K|\widehat{H}|^2\,dk\,dl\right], \qquad (27)$$

which is $1.2(\kappa_h + A_h)\mathrm{mW\ m}^{-2}$ for the present parameters. The energy loss from the geostrophic flow is thus a very significant component of the total energy dissipation, particularly in regions of small free-stream velocity (e.g. $2\mathrm{cm\ s}^{-1}$; figure 1a).

The energy deposition from the wave flow is shown by the solid curves in figure 1. The corresponding wave energy flux for each case is shown in figure 2. Both the magnitude and decay depth of the energy flux increases with free stream speed as wave generation occurs at larger scales. For $U = 2\mathrm{cm\ s}^{-1}$ the

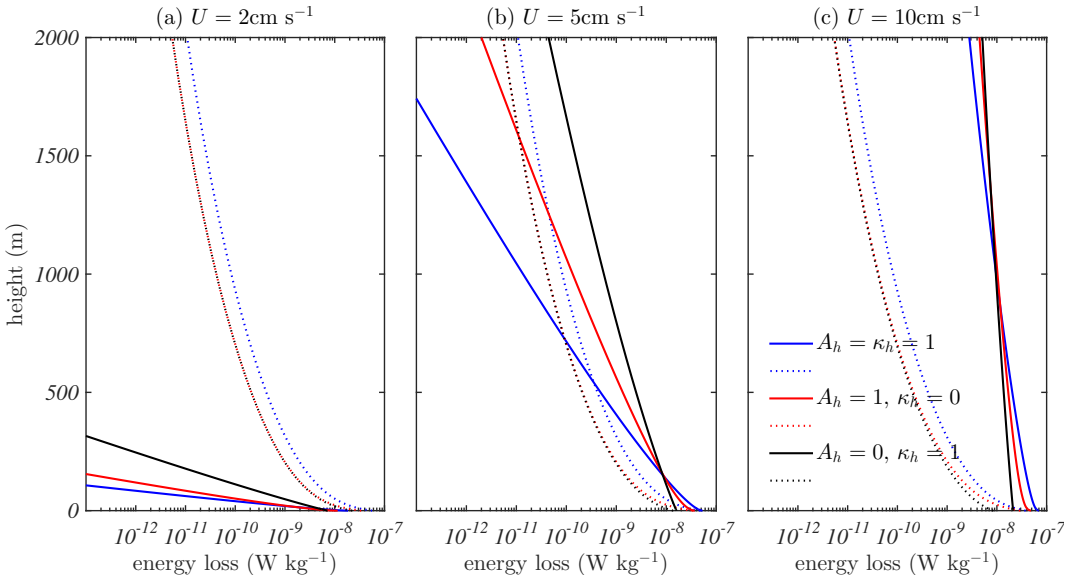


Figure 1: The total energy loss from the wave (solid) and geostrophic (dotted) flow for three choices of diffusivity/viscosity (see legend; units m$^2$ s$^{-1}$) and three free-stream speeds: (a) 2cm s$^{-1}$, (b) 5cm s$^{-1}$ and (c) 10cm s$^{-1}$. The topographic spectrum is defined by (25) with the free parameters chosen as described in the text. The buoyancy frequency is taken as $N^2 = 10^{-6}\text{s}^{-2}$ and the Coriolis parameter as $f = -1.2 \times 10^{-4}\text{s}^{-1}$.

(small) wave energy flux (0.2 mW m$^{-2}$) decays within 100m of the boundary. For $U = 5$cm s$^{-1}$ the wave energy flux (4.3 mW m$^{-2}$) decays within 1500m of the boundary. For $U = 10$cm s$^{-1}$ the wave energy flux (33 mW m$^{-2}$) remains non-zero even at 4km above the boundary. As a consequence there is significant energy deposition at large distances from the wave source — for example, energy deposition at 4km height exceeds $10^{-9}$ W kg$^{-1}$. The decay rate of the wave energy flux is significantly less for diffusivity (black curves) compared with viscosity (red curves) of the same magnitude as a result of the majority of the wave energy being at near-inertial frequencies (which have a comparatively weak buoyancy signature and minimal APE).

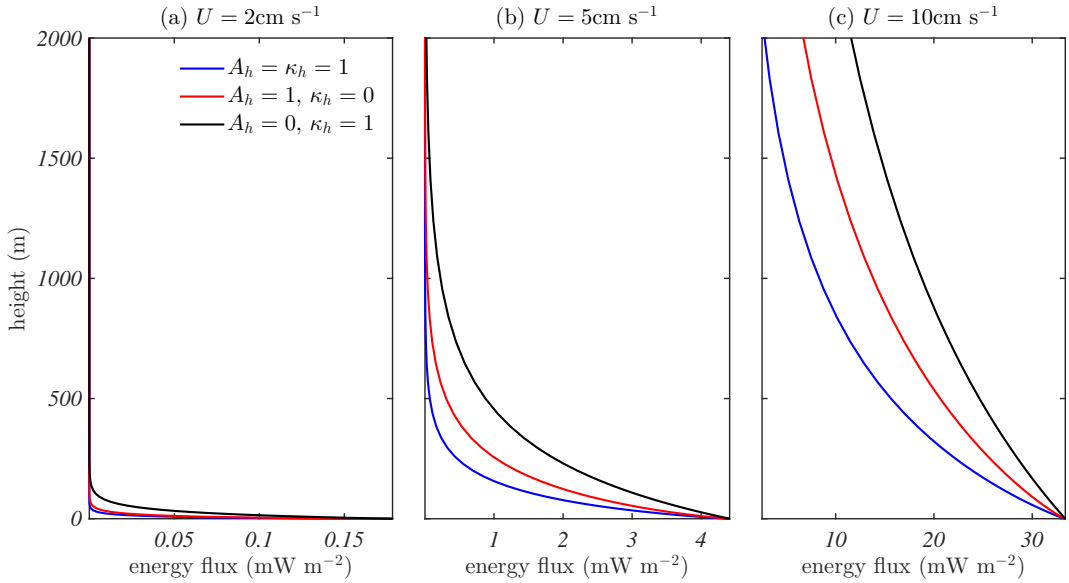


Figure 2: The wave energy flux for three choices of diffusivity/viscosity (see legend; units m$^2$ s$^{-1}$) and three free-stream speeds: (a) 2cm s$^{-1}$, (b) 5cm s$^{-1}$ and (c) 10cm s$^{-1}$. Parameter values and topographic spectrum are the same as for the previous figure.

We now compare the above solutions to the results of recent modelling studies, in particular Nikurashin et al. (2013) who use comparable parameter values ($A_h = 1$m$^2$ s$^{-1}$ and $\kappa_h \simeq 0$; red curves in figures 1 & 2). The dissipation seen in that study (e.g. figure 5a therein) is strongly enhanced near the bottom topography, O($10^{-8}$)W kg$^{-1}$, and decays rapidly to less than $10^{-9}$ W kg$^{-1}$ within a few hundred metres of the topography. This is the magnitude of dissipation predicted to come from the geostrophic non-wave flow around topography (e.g. (26) and figure 1), even in the absence of waves, and is directly proportional to the artificially elevated viscosity. The total predicted energy dissipation from the geostrophic flow is 1.2 mW m$^{-2}$ for $A_h = 1$m$^2$ s$^{-1}$, which is 20% of the reported dissipation in that study (6.1 mW m$^{-2}$;

their figure 2a). Bottom generated waves will therefore account for *at most* 4.9 mW $m^{-2}$, since there is also substantial dissipation near the ocean surface. Thus a flow speed of 5cm $s^{-1}$ (figures 1b & 2b) which corresponds to a net wave energy flux of 4.3 mW $m^{-2}$ seems to be reasonably representative of the numerical model. Figure 2b indicates that the wave energy flux reduces by over 80% within 250m of the boundary, comparable to the reported numerical model results. Only in regions of particularly strong bottom flow (e.g. 10cm $s^{-1}$; figure 2c) are the waves able to transport significant energy outside of the bottom boundary region.

The above analysis demonstrates that the dissipation seen in current generation high-resolution wave modelling studies is a direct consequence of the use of elevated horizontal viscosity/diffusivity in those models and says nothing fundamental about the energetics of internal waves in the ocean. In particular, the location of wave dissipation cannot be inferred from such models.

## 3. Discussion

Here we have described the energetics of linear waves in a fluid with elevated values of horizontal viscosity and/or diffusivity as is typical of high-resolution numerical models. In particular, we have presented extended solutions to the classical steady lee wave problem (Bell, 1975) that describe the magnitude of energy deposition and decay of the wave energy flux due to elevated horizontal viscosity and/or diffusivity. These solutions have important consequences for the modelling of internal waves.

Firstly, our solutions are vital in interpreting recent numerical model results. Ocean observations clearly show enhanced viscous dissipation near

the ocean surface and near the ocean bottom, with the bottom dissipation strongly enhanced in regions of rough topography (Waterhouse et al., 2014). This dissipation is thought to be associated with intense diapycnal mixing and hence these regions are important to sustaining the ocean overturning circulation (Wunsch and Ferrari, 2004). Recent wave-resolving model results (Nikurashin et al., 2013) have been interpreted as suggesting this enhanced dissipation is the direct result of locally generated lee waves. However, here we have shown that the dissipation local to rough topography in such models is a direct and artificial result of the subgrid parameterisations used in those models. Indeed, our theoretical result is supported by recent observational studies (Waterman et al., 2013) which report that dissipation near topography is only 2-20% of the theoretical lee wave energy flux. The present generation of high-resolution models thus provide no evidence for local lee wave dissipation near topography, and should not be used to identify where boundary generated waves will ultimately dissipate.

The solutions presented herein also suggest design criteria for future wave-resolving numerical models. In most models an artificially high viscosity and/or diffusivity is required to prevent the collapse of flow structures below the gridscale. Given that diffusivity has a smaller spurious effect on the wave field, our first suggestion is that models focusing on wave dynamics use elevated diffusivity rather than viscosity. Secondly, the viscous lee wave theory may be used to determine the maximum magnitude of horizontal diffusivity permitted to limit the spurious decay of the wave field to a certain value. For example, figure 3 shows the fraction of steady lee wave energy flux remaining at the 'ocean surface' (4km height) as a function of horizontal

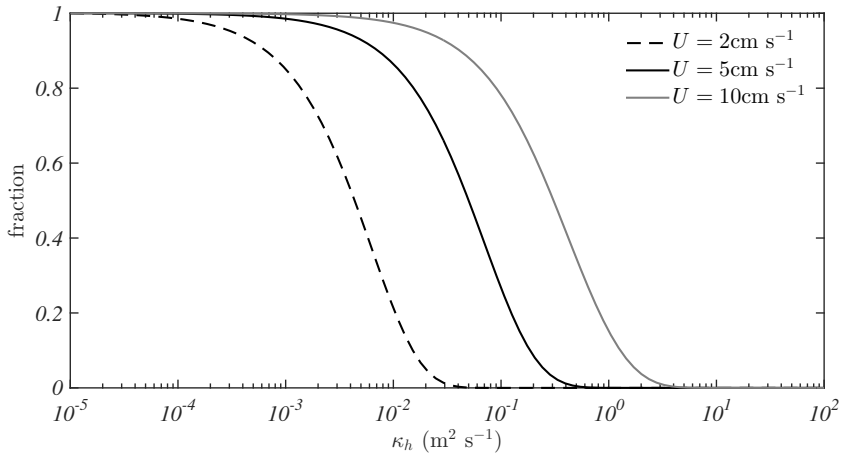


Figure 3: The fraction of the initial steady lee wave energy flux remaining at a vertical height of 4km above the bottom as a function of horizontal diffusivity $\kappa_h$, for three free-stream speeds $U$ (see legend). Parameter values and topographic spectrum are the same as for the previous figures.

diffusivity for three flow speeds and the Southern Ocean parameters described in §2. The most significant lee wave generation typically occurs for speeds exceeding 5 cm s$^{-1}$; for less than 10% dissipation at this speed over the ocean depth the horizontal diffusivity would need to be O(0.01)m$^2$ s$^{-1}$. Achieving such values seems impractical for regional ocean models since it is likely to require O(1)m horizontal model resolutions (versus the O(100m) resolution currently used). An alternative model design that would reduce, but not eliminate, spurious wave decay is to have elevated diffusivity near the model boundaries (where flow gradients tend to collapse towards the gridscale), but an essentially inviscid and adiabatic interior — we will present results from such a model in a future paper.

Internal waves play an important role in the ocean energy budget, and resolving their effect in regional ocean models is a laudable objective. However,

the viscous lee wave theory outlined here indicates that careful consideration is required before we can infer dissipation and mixing from such models.

Bell, T., 1975. Topographically generated internal waves in the open ocean. J. Geophys. Res. 80 (3), 320–327.

Danioux, E., Vanneste, J., Klein, P., Sasaki, H., 2012. Spontaneous inertia-gravity-wave generation by surface-intensifed turbulence. J. Fluid Mech. 699, 153–1732.

Goff, J. A., Jordan, T. H., 1988. Stochastic modeling of seafloor morphology: Inversion of sea beam data for second-order statistics. J. Geophys. Res. 93 (B11), 13589–13608.

Nagai, T., Tandon, A., Kunze, E., Mahadevan, A., 2015. Spontaneous generation of near-inertial waves by the Kuroshio Front. J. Phys. Oceanogr. 45 (9), 2381–2406.

Nikurashin, M., Ferrari, R., 2010. Radiation and dissipation of internal waves generated by geostrophic motions impinging on small-scale topography: Theory. J. Phys. Oceanogr. 40 (5), 1055–1074.

Nikurashin, M., Ferrari, R., Grisouard, N., Polzin, K., 2014. The impact of finite-amplitude bottom topography on internal wave generation in the southern ocean. J. Phys. Oceanogr. 44 (11), 2938–2950.

Nikurashin, M., Vallis, G. K., Adcroft, A., 2013. Routes to energy dissipation for geostrophic flows in the Southern Ocean. Nature Geosci. 6 (1), 48–51.

Polzin, K. L., 2010. Mesoscale eddy-internal wave coupling. Part II: energetics and results from PolyMode. J. Phys. Oceanogr. 40, 789–801.

Polzin, K. L., Lvov, Y. V., 2011. Toward regional characterizations of the oceanic internal wavefield. Rev. Geophys. 49 (4).

Rosso, I., Hogg, A. M., Kiss, A. E., Gayen, B., 2015. Topographic influence on sub-mesoscale dynamics in the Southern Ocean. Geophys. Res. Lett. 42 (4), 1139–1147.

Shakespeare, C. J., Taylor, J. R., 2016. Spontaneous wave generation at strongly strained density fronts. J. Phys. Oceanogr. doi:10.1175/JPO-D-15-0043.1, in press.

St Laurent, L., Garrett, C., 2002. The role of internal tides in mixing the deep ocean. J. Phys. Oceanogr. 32, 2882–2899.

Vanneste, J., 2013. Balance and spontaneous wave generation in geophysical flows. Annu. Rev. Fluid Mech. 45, 147–172.

Waterhouse, A. F., MacKinnon, J. A., Nash, J. D., Alford, M. H., Kunze, E., Simmons, H. L., Polzin, K. L., St. Laurent, L. C., Sun, O. M., Pinkel, R., et al., 2014. Global patterns of diapycnal mixing from measurements of the turbulent dissipation rate. J. Phys. Oceanogr. 44 (7), 1854–1872.

Waterman, S., Naveira Garabato, A. C., Polzin, K. L., 2013. Internal waves and turbulence in the Antarctic Circumpolar Current. J. Phys. Oceanogr. 43 (2), 259–282.

Watson, K. M., West, B. J., Cohen, B. I., 1976. Coupling of surface and internal gravity waves: a mode coupling model. J. Fluid Mech. 77 (01), 185–208.

Wunsch, C., Ferrari, R., 2004. Vertical mixing, energy and the general circulation of the oceans. Annu. Rev. Fluid Mech. 36, 281–314.